

REQA: Coarse-to-fine Assessment of Image Quality to Alleviate the Range Effect

Bingheng Li, and Fushuo Huo

Abstract—Blind image quality assessment (BIQA) of user generated content (UGC) suffers from the range effect which indicates that on the overall quality range, mean opinion score (MOS) and predicted MOS (pMOS) are well correlated; focusing on a particular range, the correlation is lower. The reason for the range effect is that the predicted deviations both in a wide range and in a narrow range destroy the uniformity between MOS and pMOS. To tackle this problem, a novel method is proposed from coarse-grained metric to fine-grained prediction. Firstly, we design a rank-and-gradient loss for coarse-grained metric. The loss keeps the order and grad consistency between pMOS and MOS, thereby reducing the predicted deviation in a wide range. Secondly, we propose multi-level tolerance loss to make fine-grained prediction. The loss is constrained by a decreasing threshold to limit the predicted deviation in narrower and narrower ranges. Finally, we design a feedback network to conduct the coarse-to-fine assessment. On the one hand, the network adopts feedback blocks to process multi-scale distortion features iteratively and on the other hand, it fuses non-local context feature to the output of each iteration to acquire more quality-aware feature representation. Experimental results demonstrate that the proposed method can alleviate the range effect compared to the state-of-the-art methods effectively.

Index Terms—Blind image quality assessment, range effect, coarse-to-fine assessment, feedback hierarchy

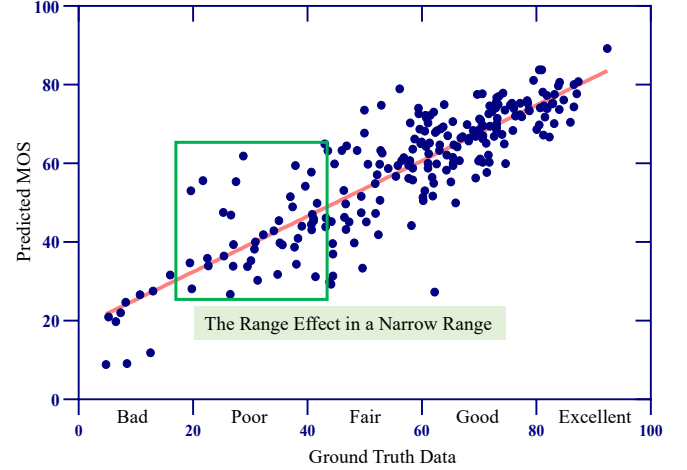
I. INTRODUCTION

IMAGE quality assessment (IQA) explores how to imitate human beings to automatically assess image quality. Accurately describing the quality change has extensive applications in image restoration, image retrieval and image quality monitoring systems, etc. IQA approaches can be generally divided into three categories: full-reference IQA approach (FR-IQA), reduced-reference approach (RR-IQA) and blind IQA approach (BIQA). FR-IQA and RR-IQA measure the similarity between the distorted image and reference image [3], [18], [20]–[23]. However, in most authentic scenarios, it is hard to achieve ideal reference information. BIQA does not require any reference image as a prerequisite in predicting the perceptual quality, so it attract great attention in recent years.

Early BIQA methods [7]–[10], [38], [40], [44]–[50], [52]–[55], [57]–[60], [62]–[64], [75] mainly focus on synthetically distorted databases [25]–[29], which consists multiple distortions generated from limited scenarios. Since images

B. Li is with the Visual Information Processing Laboratory, School of Electronic Engineering, Xidian University, Xian 710071, China and also with the Huawei Technologies Co.Ltd., Hangzhou 310000, China. (email: bhlee@stu.xidian.edu.cn).

F. Huo is with the Department of Computing, The Hong Kong Polytechnic University, Hong Kong (e-mail: fushuo.huo@connect.polyu.hk).



(a) Visualization of the predicted results of DBCNN [56] on CLIVE [30]

Scale Difference	0	1	≥ 2		
Statistic Result	139	90	3		
Distance Difference	[0,2.5]	[2.5,5]	[5,7.5]	[7.5,10]	≥ 10
Statistic Result	54	28	36	28	66

(b) Statistics results of the prediction of DBCNN [56] on CLIVE [30]

Fig. 1: (a) depicts **The range effect** as on the overall quality range, MOS and predicted MOS seem well correlated; focusing on a particular range (e.g. points within green box), the correlation is lower. (b) illustrates the statistic results of the scale difference and the distance difference between pMOS and MOS on the authentic database.

captured in the real world suffer from ever-changing contents and more complicated distortions, accurately predicting their quality remains a challenge. To deal with this problem, in recent years, some BIQA methods [56], [65], [67], [69]–[73] have been proposed with exploring novel learning strategies and leveraging complicated feature representation.

As is illustrated in Fig.1, these approaches are confronted with a common drawback that they cannot perform well on a narrower quality range, although achieving relatively high correlations spanning a wide range from extremely bad to good on challenge datasets [30]–[32]. This is illustrated in Fig.1(a), and is referred as the range effect [1], [2], [33].

How well BIQA methods perform on a narrower quality range is important for more realistic prediction on user generated content(UGC). According to [34], the distributions of image quality in the authentically distorted databases is

narrower and peakier as compared to those synthetic ones, as most pictures captured in the real world are improved by imaging device. According to the distribution property, streaming media server can screen the images with extreme qualities to obtain images with moderate qualities. These images will be integrated as the benchmark of subsequent image enhancement and image-effect synthesis. Thus, user generated content requires that BIQA model possesses more fine-grained perception to image quality. That is, it can deal with the range effect very well.

The ground truth data of the authentically distorted databases is in the form of the mean opinion score (MOS) that is the average of quality ratings given by multiple subjects. Based on this, it can be divided into five categorical scales [11]. We make statistic analysis of the scale difference and the distance difference between the predicted MOS (pMOS) and MOS. Firstly, as is shown in the first table of Fig.1(b), quality perceptual deviation from a wide range brings outliers to a scale, which destroy the prediction performance in this scale. The reason for this is that the objective BIQA model fails to keep the prediction sequence in the order as the ground truth sequence possesses. Secondly, as is shown in the second table of Fig.1(b), the predicted values can not concentrate in smaller deviation ranges, which is further intensifies the poor accuracy in the local range. Next, we aims to fix these two problems responsible for the range effect utilizing coarse-grained metric and fine-grained prediction respectively.

In response to the first problem, metric learning can be introduced to acquire the scale membership. The state-of-the-art metric learning methods map the samples into the multi-dimensional feature vectors, as for clustering or nearest neighbor classification utilizing a distance function that capture pair-wised similarity [37] [36]. This is effective on BIQA approaches for the synthetic task [38] [39] [40]. These methods map the synthetically distorted images into the feature vectors which represent distortion classification or distortion level. Based on these degradation, they can accurately metric the quality differences between pair-wised images. However, in authentic databases, images possess nonidentical scenes and immeasurable distortions that increase the difficult to obtain the coherence of feature distributions [31]. Even it can be achieved between a pair of images, it may not be quality-aware. In this paper, the proposed method maps a set of images to supervised scores. Based on these scores, rank-and-gradient metric can be conducted as for reducing the prediction deviation from a wide range and further alleviate the order confusion of the predicted quality sequence.

To deal with the inaccuracy problem in smaller deviation ranges, we adopts a multi-stage prediction strategy. Previous BIQA approaches adopt a one-time strategy to predict MOS, with a feedforward structure. However, the way neglects feedback mechanism of human visual system (HVS) as is important for perceptual learning [41]. Neurologically speaking, feedforward hierarchy underlies implicit processing for initial vision at a glance, and feedback connections add details to explicit vision with scrutiny [42]. The same applies to BIQA that fine-grained cognition of image quality is achieved through a feedback processing where high-level and low-

level features are recurrently integrated by HVS. Moreover, feedback-based learning approach has been proved more effective than the commonly employed feedforward paradigm in prediction tasks [?]. In the proposed method, MOS prediction is constantly refined under multi-level tolerance constraints through a feedback structure. Besides, coarse-grained metric is fused into the structure as the prior knowledge as it is easier compared to fine-grained prediction from the perspective of curriculum learning [68].

Patrick et al. [24] have already proposed a new evaluation criterion aiming at FR-IQA which is less dependent on the range effect. However, there has been no way to solve this problem in BIQA yet. To deal with this challenge, we first propose a novel coarse-to-fine assessment method. The flowchart of the proposed method is illustrated in Fig.2. Firstly, it takes a set of images as input. The set contains a predicted image and four anchors sampled from different quality scales randomly. And then, these images are mapped into multi-scale distortion features and context features. The former are taken as the input of feedback blocks and the latter are fused into the outputs of feedback blocks in each time step. Based on this, coarse-to-fine assessment acquires local-to-global feature representation which is more quality-aware [70]. Finally, after feature mapping, coarse-to-fine assessment is conducted. In the first time step, coarse-grained metric utilizes rank-and-gradient loss to keep the order and grad of predicted sequence consistent with the ground data. In subsequent time steps, fine-grained prediction adopts multi-level tolerance losses to refine the prediction accuracy.

II. RELATED WORK

In this section, we review BIQA methods for synthetically distorted images and BIQA methods for authentically distorted images respectively.

A. BIQA for Synthetically Distorted Images

In the previous development, the research of BIQA approaches for synthetic task mainly follows two kinds of ideas: traditional methods and learning-based methods.

Commonly traditional BIQA approaches first extract hand-crafted features based on the empirical analysis and then adopt a regression function to map the features into quality score. The most famous type methods is the one based on the characteristics of natural statistical scenes (NSS), such as DIIVINE [44], BLIINDS-II [45] and BRISQUE [46]. This type of methods assumes that natural images have certain statistical properties affected by the distortion, which makes the image look unnatural. Therefore, features can be extracted from frequency, spatial and wavelet domain based on the statistical properties of an image to predict its quality score. In addition, there are also some other methods based on human visual system (HVS), such as NRSL [47], LPSI [48], M3 [49] and RISE [50]. These methods utilize HVS to construct the quality aware features, assuming that HVS is adapted to the structure information. However, theses hand-crafted features are time-consuming and meantime lack of

generalization ability due to the diversity of image contents and distortions.

Unlike the traditional BIQA methods, the learning based BIQA approaches automatically generate the quality-aware features. In the early stage, CBIQ [51] and CORNIA [52] introduce the codebook feature based learning into BIQA. These methods first utilize raw image patches extracted from a set of unlabeled images to learn a dictionary in unsupervised manner, and then encode the test images on the dictionary to obtain the feature representations for quality estimation. In the subsequent development, CNN pushes the significant development of BIQA thanks to its powerful learning ability. Kang et al. [53] propose a shallow CNN network which performs the mapping progress from a predicted image to its perceptual quality. WaDIQaM [54] propose a significantly deeper framework which comprises ten convolutional layers and five pooling layers for feature extraction, and two fully connected layers for regression. As these networks grow deeper and wider, they need larger and larger annotated databases for training. Due to extremely labor-intensive and costly subjective-experiment, the current IQA databases are too small to meet this requirement.

To deal with the small sample problem, it needs to explore more effective learning strategies and leverage more complicated features. Some methods find a way out in the transfer learning. MEON [55] and DBCNN [56] pretrain a classification model on a large-scale synthetic database to acquire the initialized network parameters which are, to some extent, distortion aware. RankIQA [40] and dipIQ [57] propose a pairwise learning-to-rank (L2R) algorithm. With it, they can learn to rank image in terms of image distortion. Then they transfer the prior knowledge learned from ranked images to a traditional CNN. After fine-tuning it on IQA databases, it can improve the accuracy of IQA. RRLRIQA [58] make further exploration and model the BIQA as a Markov decision process to optimize the whole image-quality ordering directly. L2R effectively improves the performance of these CNN-based methods.

Since human are the ultimate receivers of images, the properties of human visual system (HVS) should also be modeled in a data-driven manner. Perceptual error map is learned to guide quality prediction in [59] [60] where DeepQA [59] is designed from FR-IQA methods and BPSQM [60] utilize the U-Net [61] to generate the similar map of the distorted image for reference. In HVS-Net [62], visual saliency and just noticeable difference (JND) [81] are taken into account to acquire the perceptually important features. Meantime, the rank loss is proposed to penalize the model when the order of its predicted quality scores is biased against that of the ground truth scores.

Some GAN-based methods have also been developed in the last few years. H-IQA [63] and RAN4IQA [64] suppose that HVS unveils the mask of distortion and recreates a hallucinated scene without distortion in mind. In addition, AIGQA [75] propose an active inference module based on the generative adversarial network (GAN) to predict the primary content. Since these IQA methods have achieve great improvement in synthetically distorted databases, a drawback exists

when applied into authentic ones. The reference information is inevitable utilized in their training stage, which makes them limited in user generated content (UGC) due to the lack of reference images.

B. BIQA for Authentically Distorted Images

Most BIQA methods focus on the synthetically distorted images, but relatively few approaches have been proposed on the more challenging problem of authentic IQA. In recent years, based on the multiple learning strategies, some methods are proposed to cope with this challenge. BLINDER [65] and DBCNN [56] pretrain a classification model on a photographically generated classification databases such as ImageNet [66] to acquire the quality-aware network parameters, which can help the regression task in IQA databases. MetaIQA [67] adopts model-agnostic meta-learning (MAML) [14] to learn the prior knowledge among different synthetic distortions. However, due to the imbalance between the synthetic distortion and the authentic distortion, the learned knowledge cannot be generated effectively to the authentically distorted IQA databases, which is obvious in the experiment results. SFA-IQA [69] and HyperIQA [70] make IQA model understand the content diversity in authentic databases, the former utilizing semantic feature aggregation (SFA) to eliminate the impact of image content variation and the latter utilizing a hyper network architecture to evaluate the image quality adaptively according to the image content. In NAR-CNN [71], the authors propose a dual-path network to support IQA from reference image with similar scene but is not aligned. Considering the fact that an image receives divergent subjective scores from different human raters, PQR [72] and DeepRN [73] utilize the distribution of subjective scores to describe image quality.

In this paper, as for the unanswered range effect in BIQA of UGC, REQA is proposed to fix it. Compared to the state-of-the-art methods, REQA can effectively tackle the prediction deviation in narrow ranges on the authentic databases which contain images close to user generated content.

III. PROPOSED METHOD

By alleviating the range effect to improve the prediction performance in a narrow quality range, a novel BIQA method (named as REQA) is proposed. As is illustrated in Fig.2, REQA is end-to-end, dividing and conquering the BIQA task to multi-time steps to realize the coarse-to-fine image quality assessment. REQA is realized by a feedback structure. As for more quality-aware feature representation, we add a Transformer Encoder [15] in REQA to obtain the non-local features. Following, we first introduce the coarse-to-fine assessment and then discuss the net framework from two aspects: the backbone feedback network for multi-scale distortion perception and the Transformer Encoder for context understanding.

A. Coarse-to-Fine Assessment for the range Effect in IQA

The proposed method employs a multi-time strategy $t \in \{1, 2, \dots, T\}$ where feedback mechanism controls the progress of BIQA task. In particular, it captures multi-scale quality-aware features, and then they are integrated and mapped into

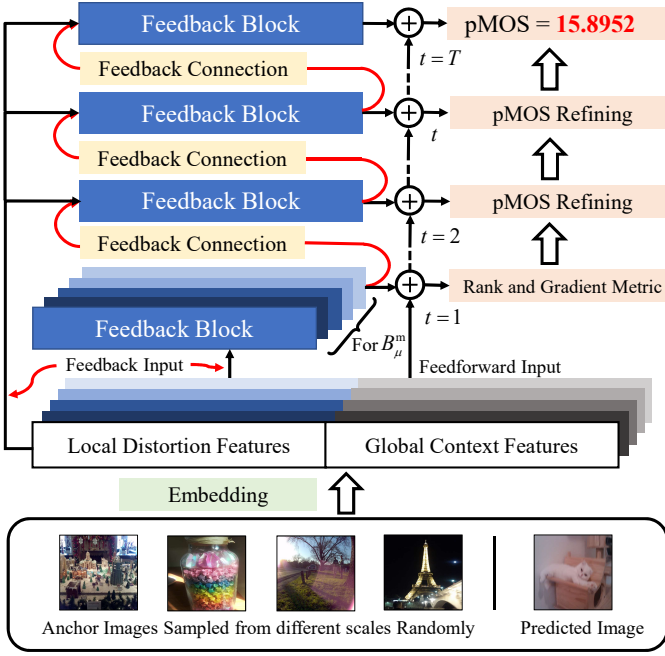


Fig. 2: Flowchart of the proposed REQA. REQA adopts a feedback hierarchy to realize coarse-to-fine quality assessment within multiple time steps. Here, rank-and-gradient metric accomplishes coarse-grained assessment and multi-stage pMOS refinements complete fine-grained assessment. In addition, REQA integrates image feature representations from two aspects, where the first is to process multi-scale distortion features through iteration and the second is the fusion of context features from Transformer Encoder [15].

the quality score that is finally utilized by each time step to accomplish the assessment subtask. The whole assessment process is coarse-to-fine, containing coarse-grained metric and fine-grained prediction.

1) *Coarse-grained metric*: As for coarse-grained metric, the proposed method redesigns the sample strategy of training data. We randomly sample a mini-batch with K 2-tuples $B = \{(I_k, s_k)\}_{k=1}^K$ from current training set. Here, I_k and s_k are the training images and MOS labels, respectively. This randomly sampled mini-batch contains training samples from multiple quality scales. Coarse-grained metric aims to improve the perception of quality difference, so we group the training samples to form a micro-batch $B_\mu^m = \{(I_i, s_i)\}_{i=1}^5$ where a predicted image and four anchors are sampled from five different quality scales. Here, $m \in [1, M]$ where $M = \lfloor K/5 \rfloor$. Compared to the state-of-the-art ones [56] [69] [70] [72], the sample strategy has two advantages as it can be adaptive to the metric task and moreover it can fix the small sample problem in BIQA because of the combinatorial diversity.

The realization of coarse-grained metric is based on the quality ranking and gradient keeping, which occupies the first-time step of feedback learning as the prior knowledge of fine-grained prediction. Different from [62], the proposed method puts forward a loss which can not only metric quality order but also keep the distance difference of pairwise predicted scores consistent with the one of respective ground truth scores. For

I_i and I_j , rank loss is first defined as:

$$L_{t=1}^{rank}(i, j) = \max(0, \frac{-(s_i - s_j) \times (\mathcal{F}_{t=1}(I_i; \theta) - \mathcal{F}_{t=1}(I_j; \theta))}{\|s_i - s_j\|_1 + \sigma} \times (\|s_i - s_j\|_1 + 1)) \quad (1)$$

where, θ is the network parameters, $\mathcal{F}_{t=1}(I_i; \theta)$ represents the quality prediction of image i in $t = 1$ and σ is a small stability term. In our experiment, we set $\sigma = 0.0001$. When the order of pairwise prediction sequence is consistent with the ground truth order, rank loss equals to zero, otherwise it is reduced to an absolute loss as:

$$L_{t=1}^{rank}(i, j) = \|s_i - s_j\|_1 \times \|\mathcal{F}_{t=1}(I_i; \theta) - \mathcal{F}_{t=1}(I_j; \theta)\|_1 \quad (2)$$

The rank loss keeps the order consistency, and gradient loss maintains the stability of pair-wised quality distance difference as:

$$L_{t=1}^{gradient}(i, j) = \left| \|s_i - s_j\|_1 - \|\mathcal{F}_{t=1}(I_i; \theta) - \mathcal{F}_{t=1}(I_j; \theta)\|_1 \right| \quad (3)$$

Overall, for a micro batch B_μ^m , coarse-grained loss is defined as:

$$L_{t=1}^{Coarset} = \sum_{i=1}^5 \sum_{j=i+1}^5 (L_{t=1}^{rank}(i, j) + L_{t=1}^{gradient}(i, j)) \quad (4)$$

2) *Fine-grained prediction*: Fine-grained prediction is inspired by the episodic curriculum learning [68], adopting an easy-to-difficult strategy to realize $t \in [2, T]$ prediction refinement. Specifically, We set a different threshold for each time step to compute the loss, and as the feedback information is processed continually, the threshold is reduced. Overall, fine-grained loss is defined as:

$$L_t^{Fine} = \max(0, \|s_i - \mathcal{F}_{t_i}(I_i; \theta)\|_1 - l_{t_i}) \quad (5)$$

$$l_t > l_{t+1} \geq 0, t < t+1$$

where, L_t^{Fine} is the loss function in time step t , and l_t represents the threshold in t . The whole loss of the proposed method is calculated as:

$$L = w_1 L_{t=1}^{Coarset} + w_2 L_{t=2}^{Fine} + w_3 L_{t=3}^{Fine} + \dots + w_T L_{t=T}^{Fine} \quad (6)$$

$$w_1 + w_2 + \dots + w_T = 1$$

where, in our experiment, we set $T = 4$, $l_2 = 5$, $l_3 = 2.5$ and $l_4 = 0$. The values of w_1, w_2, w_3 and w_4 is dynamically adjusted with the training task going on to satisfy the curriculum learning principle. The set for w_1, w_2, w_3 and w_4 is in Section IV-A(3).

B. Feedback Network for multi-scale distortion perception

Feedback Network (FN) is the core part of the proposed method which controls the feedback process to perceive image degradation from multi-scale distortion features continually. The whole network concludes three elements as feature extraction, time-domain iteration and space-domain integration. The detail of this module is shown in Fig.3.

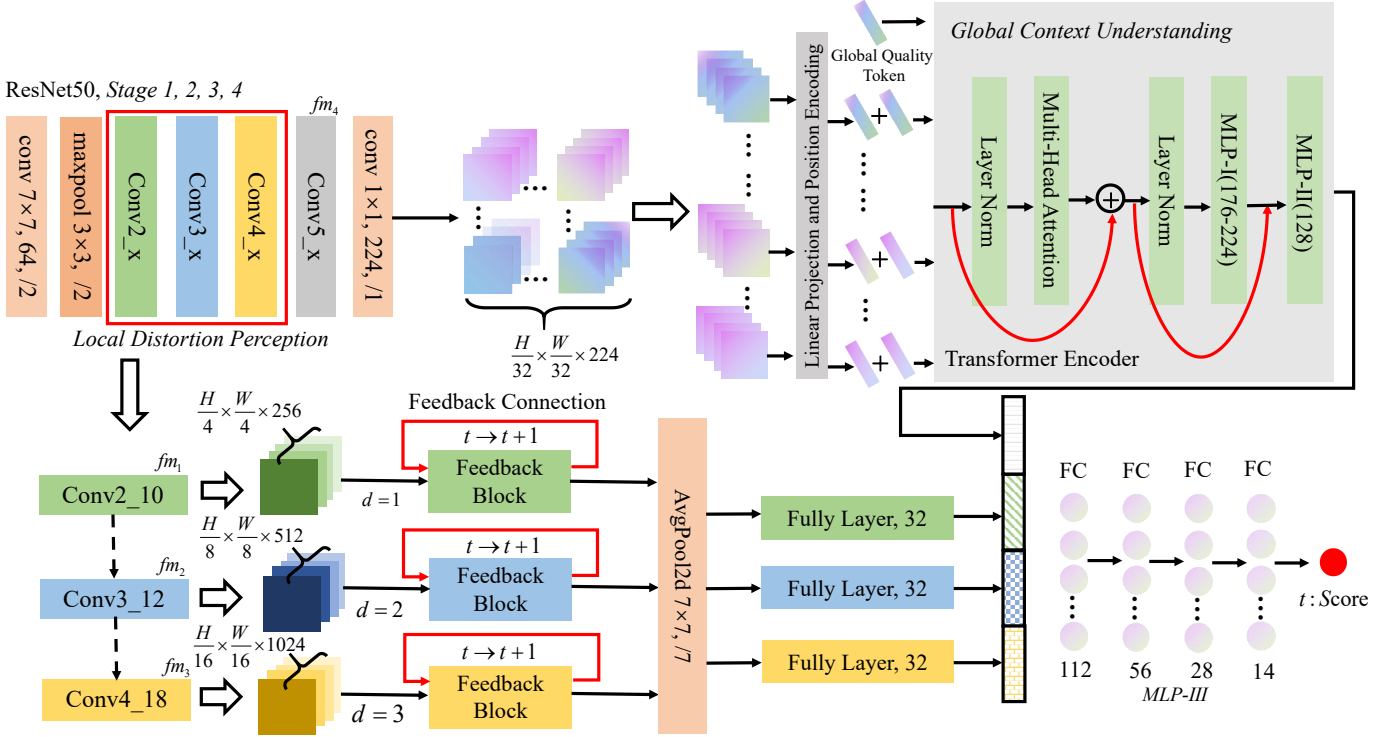


Fig. 3: The overview framework of REQA. It consists of three parts as the baseline network ResNet50 [12], feedback network (FN) and Transformer Encoder (TE). Here, as the core part of REQA, FN processes multi-scale features iteratively utilizing feedback blocks. TE provides the non-local representation for the outputs of feedback blocks in each time step. In addition, global and local representations are firstly concatenated and then mapped by multilayer perceptron(MLP-III) into a supervised score to predict image quality.

1) *Feature extraction*: Multi-scale features contain diverse low-level information, which have been proved to be effective for IQA [38] [70]. Meantime, neurology also proves that HVS can add details into distortion areas through feedback connection. The property of HVS contributes to quality perception. Thus, multi-scale features combined with feedback mechanism have greater gain for IQA. In this paper, REQA adopts a ResNet50 [12] to acquire multi-scale features. Specifically, we remove global average pooling layers and fully connected layers of ResNet50, and initialize corresponding network parameters using pretrained model in ImageNet [66]. Finally, multi-scale features fm_1, fm_2, fm_3 are extracted from *conv2_10*, *conv3_12*, *conv4_18* layers respectively.

2) *Time-domain iteration*: Local distortion perception is completed by three feedback blocks. Each block takes a single scale feature map and the feedback feature extracted from last time step as input. Through integrating and correlating these features, quality-aware representation is got to finish the assessment task of current step. For feedback block d , this iterative process is expressed as:

$$\begin{aligned} f_{o,d,t} &= \mathcal{G}_d(fm_d, fh_{d,t-1}; \phi_d) \\ d &= 1, 2, 3, t = 1, 2, \dots, T \end{aligned} \quad (7)$$

where $fh_{d,t-1}$ is hidden state in time step $t-1$, $f_{o,d,t}$ is the output in time step t , ϕ_d represents the block parameters and \mathcal{G}_d expresses the mapping function.

3) *Space-domain integration*: Space-domain integration is dependent on feedback block whose inner structure is based on ConvLSTM [13] as illustrated in Fig.4. An LSTM cell uses multiple gates to control information saving, discarding and merging, and finally uses hidden states to pass feedback through iterations. We briefly presents the connections between gates in it as:

$$\begin{aligned} f_{i,d,t} &= \sigma(W_{d,x_i} fm_d + W_{d,h_i} fh_{d,t-1}) \\ f_{g,d,t} &= \sigma(W_{d,x_f} fm_d + W_{d,h_f} fh_{d,t-1}) \\ f_{o,d,t} &= \sigma(W_{d,x_o} fm_d + W_{d,h_o} fh_{d,t-1}) \\ \tilde{f}_{c,d,t} &= \tanh(W_{d,x_c} fm_d + W_{d,h_c} fh_{d,t-1}) \\ f_{c,d,t} &= f_t^d \circ f_{c,d,t-1} + f_{i,d,t} \circ \tilde{f}_{c,d,t} \\ fh_{d,t} &= o_t^d \circ \tanh(f_{c,d,t}) \end{aligned} \quad (8)$$

where $f_{i,d,t}$ is the input gate, $f_{g,d,t}$ is the forget gate, $f_{o,d,t}$ is the output gate, $f_{c,d,t}$ is the memory cell, σ is the logistic sigmoid function, and W_* is the weight matrix of conv block. In the proposed method, according to d , we set three conv blocks whose details is also shown in Figure 4. The output $f_{o,d,t}$ is finally mapped into $v_{d,t} \in R^{1 \times 32}$.

C. Transformer Encoder for context understanding.

To some extent, the perception of the local distortion can assess the degree of image quality degradation effectively.

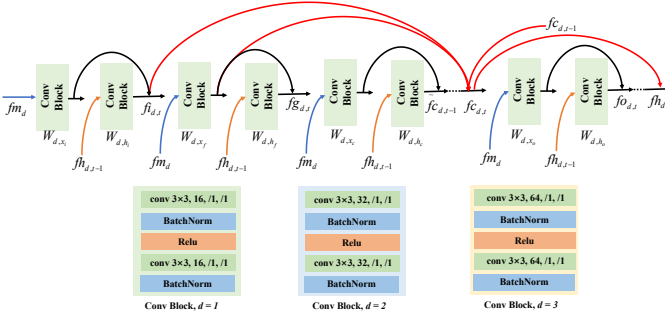


Fig. 4: Architecture details of feedback block.

However, there are still some situations where local distortion cannot be quality-aware. For example, photographers are used to throw the background out of focus as to improve visual effect of the foreground. In this case, when we only pay attention to the background and ignore its correlation with foreground, it is easily regarded as fuzzy distortion that affect the image quality. Thus, adding the context information to local feedback features contributes to understanding image quality comprehensively.

Compared to traditional CNN, Transformer [15] manages to capture long range interactions thanks to its multi-head attention mechanism, that is, it is effective to obtain non-local features of an image. Meanwhile, CNN has some inherent inductive biases, such as translation invariance, scale invariance and so on, which is not possessed by Transformer. These properties make CNN suitable for feature extraction. Therefore, in the proposed method, we adopts *ResNet50* + *Transformer* structure to acquire feedforward context feature. The details of the Transformer Encoder (TE) is illustrated in Fig.3. It consists of three elements: patch embedding, multi-head attention module and multilayer perceptron.

1) *Patch embedding*: The original distorted image $I_i \in R^{H \times W \times 3}$ is processed by *ResNet50* and respective feature map $f_{m4} \in R^{\frac{H}{32} \times \frac{W}{32} \times C}$ is acquired by *conv5_9*. Here, (H, W) is the resolution of I_i and C is the number of channels. Transformer encoder takes one-dimensional vector as input. As for this, f_{m4} is cut into N patches firstly where each patch $\mathcal{P}_{n,i} \in R^{P \times P \times C}$, $n \in [1, N]$ and $N = H \cdot W / (32^2 \cdot P^2)$. Then, $\mathcal{P}_{n,i}$ is flattened into a vector $\eta_{n,i} \in R^{1 \times P^2 C}$ which is mapped into $\zeta_{n,i} \in R^{1 \times D}$ by a learnable matrix W_{pe} as:

$$\zeta_{n,i} = \eta_{n,i} \cdot W_{pe}, W_{pe} \in R^{P^2 C \times D} \quad (9)$$

where, in the experiment, we set $D = 224$. Moreover, to keep positional information, a standard learnable position embedding $\rho_{n,i} \in R^{1 \times D}$ is added into $\zeta_{n,i}$ to obtain the embedding $\varepsilon_{n,i}$ of $\mathcal{P}_{n,i}$ as:

$$\varepsilon_{n,i} = (\zeta_{n,i} + \rho_{n,i})^T \quad (10)$$

To realize the perception of the whole quality representation, we concatenate a trainable token $\mathbf{x}_{quality} \in R^{1 \times D}$ to the patch embeddings $\{\varepsilon_{1,i}, \varepsilon_{2,i}, \dots, \varepsilon_{N,i}\}$, similar to BERT's [16] and ViT's [17] class token. Finally, the input matrix X_i is defined as:

$$X_i = [\mathbf{x}_{quality}^T; \varepsilon_{1,i}; \varepsilon_{2,i}; \dots; \varepsilon_{N,i}]^T \quad (11)$$

2) *Multi-head attention*: Continuing the traditional **qkv** idea [15], self-attention map is acquired through a weighted sum over all values V of the input matrix X_i . Each element in the weighting matrix A are the pairwise correlation between two patch representations in X_i which is calculated by the dot product of respective query and key. The specific computational process is as:

$$\begin{aligned} [Q, K, V] &= \mathcal{L}(X_i)W_{sa}, W_{sa} \in R^{D \times 3D_h} \\ A &= \text{softmax}\left(\frac{QK^T}{\sqrt{D_h}}\right), A \in R^{(N+1) \times (N+1)} \\ S(X_i) &= AV \end{aligned} \quad (12)$$

where $\mathcal{L}(\cdot)$ denotes layer normalization and $S(\cdot)$ is self-attention operation.

Multi-head attention utilizes multiple self-attention operations to integrate global context relevance from local patch embeddings. Here, we set D/D_h self attentions as:

$$\mathcal{M}(X_i) = \mathcal{L}([S(X_1); S(X_2); \dots; S(X_{D/D_h})]W_{ma} + X_i) \quad (13)$$

where $W_{ma} \in R^{D \times D}$ is the transition matrix.

3) *Multilayer perceptron*: We extract a 1D vector $\xi_{quality}$ from $\mathcal{M}(X_i)$ which is corresponding to $\mathbf{x}_{quality}$. And then MLP-I takes $\xi_{quality}$ as the input to obtain $\tilde{\xi}_{quality}$. After MLP-II processing $\tilde{\xi}_{quality}$, \mathbf{v}_m is computed. Finally, through feature concatenating and mapping, $\mathcal{F}_t(I_i; \theta)$ is achieved as:

$$\mathcal{F}_t(I_i; \theta) = \text{MLP} - \text{III}(\mathbf{v}_m \oplus \mathbf{v}_{1,t} \oplus \mathbf{v}_{2,t} \oplus \mathbf{v}_{3,t}) \quad (14)$$

where \oplus represents concat operation.

IV. EXPERIMENT

In this section, we first introduce the experimental protocols, including databases, criterion and implementation details. Then we compare REQA with the state-of-the art BIQA methods from global and local prediction performance respectively. We next implement a series of ablation experiments to verify the contribution of different components of REQA. Finally, we also present some visualization samples acquired from local distortion perception module to verify the effectiveness of the feedback hierarchy.

A. Experiment Protocols

1) *Databases*: Three authentically distorted IQA databases including CLIVE [30], KonIQ-10k [31], and BID [32] are used to evaluate the performance of proposed method. CLIVE contains 1162 images captured from many diverse mobile devices under the real-world conditions. KonIQ consists of 10073 images, selected from 10 million YFCC100M entries. The sampling strategy of it concerns the authenticity of distortions, the diversity of content, and quality-related indicators. BID comprises 586 images with realistic blur distortions such as motion blur and defocusing blur, etc.

These databases are constructed based on quality rating, i.e., bad, poor, fair good, and excellent. Crowdsourcing strategy utilizes subjects to give multiple quality ratings to single image. These ratings is then rescaled into $[1, 100]$ to compensate for the biases of individual evaluations. Here, the higher

score corresponds to the higher quality. Trough averaging them, MOS/DMOS is obtained as the quality label. In our experiment, because these three databases provide no original category labels, we divide the ground truth data according to Absolute Category Rating(ACR) [11] into five equal potions as Excellent (80 – 100), Good (60 – 80), Fair (40 – 60), Poor (20 – 40) and Bad (0 – 20) as for local prediction performance experiment.

2) *Criterion*: In our experiments, the Sperman Rank Order Correlation Coefficient (SROCC) and the Pearson Linear Correlation Coefficient (PLCC) are applied to evaluate the performance of BIQA methods. SROCC is to measure the monotonicity between the ground truth data and the prediction scores. PLCC is to evaluate the linear correlation between these two. Given N images, the SROCC is defined as:

$$SROCC = 1 - \frac{6 \sum_{i=1}^N d_i^2}{N(N^2 - 1)} \quad (15)$$

where, d_i is the rank difference between MOS and pMOS of the i – th image. And PLCC is computed as:

$$PLCC = \frac{\sum_{i=1}^N (s_i - \mu_{s_i})(\tilde{s}_i - \mu_{\tilde{s}_i})}{\sqrt{\sum_{i=1}^N (s_i - \mu_{s_i})^2} \sqrt{\sum_{i=1}^N (\tilde{s}_i - \mu_{\tilde{s}_i})^2}} \quad (16)$$

where s_i and \tilde{s}_i denotes MOS and pMOS of the i – th image, and μ_{s_i} , $\mu_{\tilde{s}_i}$ correspond to the mean of each.

3) *Implement Details*: We conducted training and testing using Pytorch on a NVIDIA 2080Ti GPU. In the proposed model, all the training images are randomly cropped to 224×224 pixel patches. The results are obtained from 20 train-test iterations. In each iteration, we randomly select 80% images for training, and the remaining 20% for testing, so there is no overlap between the training set and the test set. We train our model using Adam [5] optimizer with weight decay $5e-4$ for 40 epochs. Learning rates for the backbone ResNet50 and the other modules are first set to $2e-5$ and $2e-4$ respectively, and reduced by 10 in 10 th epoch, 20 th epoch, and 30 th epoch respectively.

In addition, the setting for w_1 , w_2 , w_3 and w_4 is consistent with the episodic curriculum learning [68]. First of all, we prioritize the assessment tasks corresponding to w_1 , w_2 , w_3 and w_4 in Eq.6 based on the easy-to-difficult strategy. Specifically, coarse-grained metric occupy the highest priority; meantime, fine-grained loss with bigger threshold possesses higher priority. In addition, we divide the training into four stages, with ten epoches for each stage. Finally, the setting is $w_1 = 0.25$, $w_2 = 0.5$, $w_3 = 0.25/3$, $w_4 = 0.25/3$ in stage 1, $w_2 = 0.5$, $w_3 = 0.25$, $w_4 = 0.25$ in stage 2, $w_2 = 0.25$, $w_3 = 0.5$, $w_4 = 0.25$ in stage 3 and $w_1 = 0.25$, $w_2 = 0.25$, $w_3 = 0.25$ and $w_4 = 0.5$ in stage 4.

B. Global Prediction Performance Experiment

In this section, we first conduct experiments in individual authentically distorted databases to verify the effectiveness of the proposed method and then we make statistic significant test to validate the robustness of REQA.

TABLE I: Global prediction performance on authentically distorted databases CLIVE [30], KonIQ [31] and BID [32]. The best two results are highlighted in bold.

IQA methods	CLIVE		BID		KonIQ-10K	
	SROCC	PLCC	SROCC	PLCC	SROCC	PLCC
BRISQUE [46]	0.608	0.629	0.562	0.593	0.665	0.681
ILNIQE [78]	0.432	0.508	0.516	0.554	0.507	0.523
HOSA [77]	0.640	0.678	0.721	0.736	0.671	0.694
BIECON [79]	0.595	0.613	0.539	0.576	0.618	0.651
WaDIQAM [54]	0.671	0.680	0.725	0.742	0.797	0.805
SFA [69]	0.812	0.833	0.826	0.840	0.856	0.872
PQR [72]	0.857	0.882	0.775	0.794	0.880	0.884
DBCNN [56]	0.851	0.869	0.845	0.859	0.875	0.884
SGDNet [80]	0.851	0.872	-	-	-	-
MetalQA [67]	0.802	0.835	0.825	0.828	0.850	0.887
HyperIQA [70]	0.859	0.882	0.869	0.878	0.906	0.917
AIGQA [75]	0.751	0.761	-	-	-	-
REQA	0.865	0.880	0.874	0.886	0.904	0.916

TABLE II: Statistic significance test results on CLIVE [30].

	MetalQA	AIGQA	DBCNN	HyperIQA	REQA
MetalQA [67]	0	-1	-1	-1	-1
AIGQA [75]	1	0	-1	-1	-1
DBCNN [56]	1	1	0	-1	-1
HyperIQA [70]	1	1	1	0	0
REQA	1	1	1	0	0

1) *Single database evaluations*: We compare the proposed REQA with 3 traditional methods and 9 DNN-based algorithms. The experimental results are exhibited in Tab.I, where the top two SROCC and PLCC are marked in bold. All the results of the traditional methods are implemented from the original codes. As for the DNN-based methods [54] [75] [69] [79] [80], the results are taken from respective papers. In the last two years, the state-of-the-art methods [56] [67] [70] [72] are raised and the experimental results of them is reproduced by the source codes released by their authors.

Compared with the traditional methods, REQA possesses notable advantage. Particularly in KonIQ, REQA achieves competitive performance, with improvement about 23% on SROCC and 22% on PLCC. It benefits from the powerful feature representation ability of DNN which can obtain more diverse degradation information to perceive the quality of the image in real world than the traditional methods can do.

When compared with DNN-based algorithms, REQA also achieves promising results on 3 databases. Specifically, REQA outperforms all the methods on BID. As for CLIVE, REQA obtains the best result on SROCC, and on PLCC, it gets top two result. On KonIQ, REQA achieves a slightly lower performance compared with HyperIQA [70] but it still gets a prominent results about 0.904 on SROCC and 0.916 on PLCC. Overall, the proposed method achieves outstanding improvement of SROCC in experiments, which suggests that the design for alleviating the range effect enhances the sensitivity to the change of image quality, thereby optimizing the order of the predicted scores. This can be further proved in Section IV-C where more statistic results is listed.

2) *Statistical significant test*: As for demonstrating that REQA possess greater robustness, we import the statistic

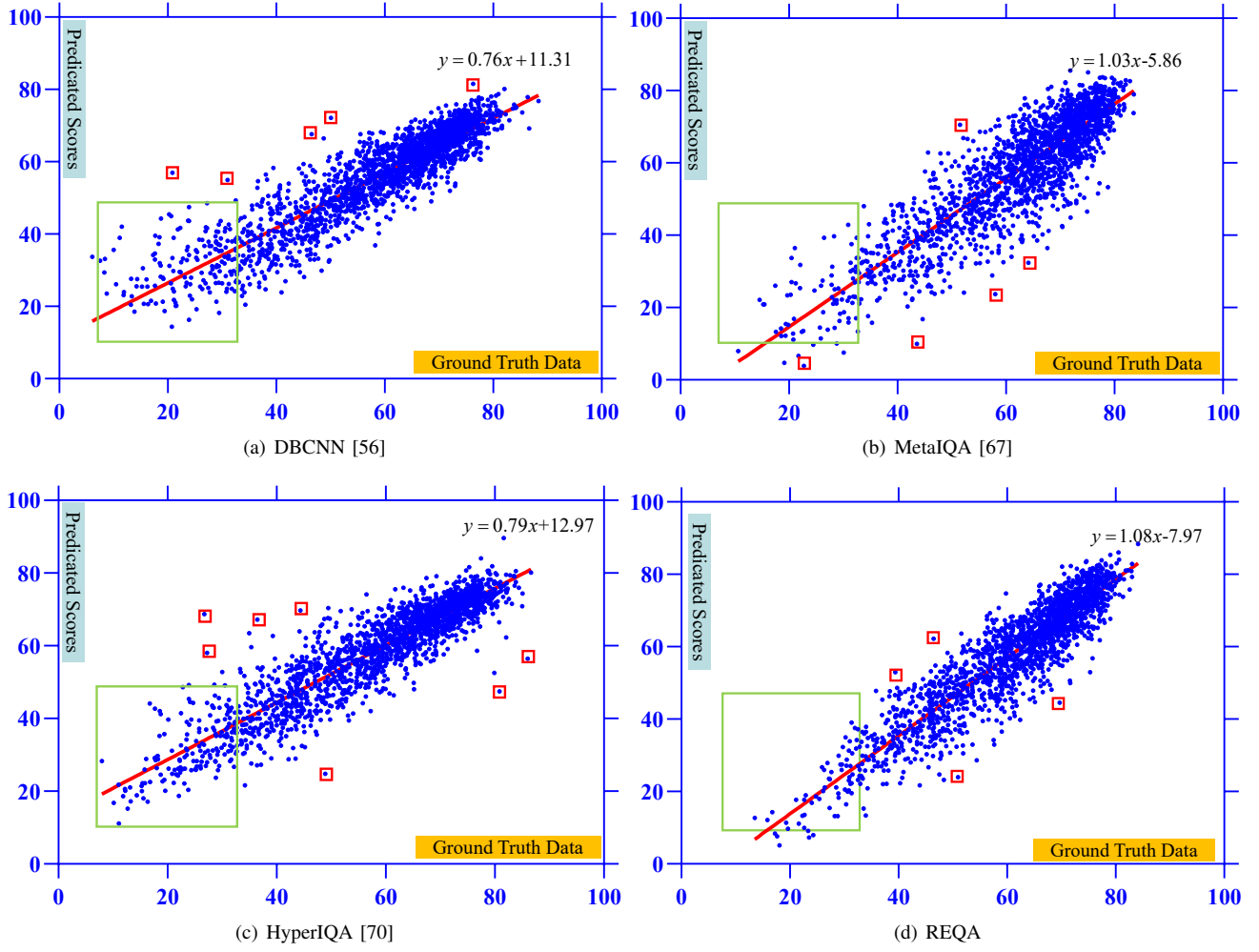


Fig. 5: Visualization of predicted results.

significance test which is conducted to verify the significance of the predicted results between each two methods. Here we choose PQR [72], DBCNN [56], HyperIQA [70], MetaIQA [67] and AIGQA [75] as comparison methods where the former three achieve the state-of-the-art performances and the latter two adopts up-to-date algorithmic logic to deal with BIQA problem. The SROCC scores of each methods when training and testing on CLIVE are utilized for the test. Experimental results are showed in Tab.II. Here, '1/-1/0' represents that the model in row is statistically better than/worse than/indistinguishable from the model in column with 95% confidence level. As we can see from Tab. II, REQA is statistically better than most methods. Compared to HyperIQA, REQA achieves an indistinguishable level. HyperIQA propose a self-adaptive method to perceive content variation which is effective to obtain the improvement of sensitivity of image quality change. Based on this, the model can assign each image with a specific weight in the training stage. Thus, it can fix the non-convex problem belonging to the authentic databases. This is the reason for its performance in statistic significance test.

C. Local Prediction Performance Experiment

In this section, we conduct the local-prediction performance experiment on KonIQ. Compared methods includes DBCNN [56], HyperIQA [70] and MetaIQA [67]. The first two methods achieves the top two performances compared to previous BIQA methods. MetaIQA adopts a up-to-date training strategy as MAML [14] does. All the methods utilize same division of the database as to keep the consistency of test samples. Results from respective best models is evaluated in each category interval. For further examining the effectiveness of REQA, we also analyze the prediction bias and the number of outliers statistically.

1) *Single interval evaluation*: As is shown in Tab.III, REQA achieves outstanding performances. Compared with the three methods, REQA gets best results in *Poor* range, *Fair* range and *Good* range. Especially in *Poor* range, REQA achieves about 20% improvement both on SROCC and PLCC in contrast to HyperIQA [70]. In *Excellent* range and *Bad* range, four methods all fails to obtain ideal results. According to statistic analysis, there are a few samples in these two ranges, which greatly increases the prediction difficulty as even a outlier leads to the obvious disturbance on SROCC. In

TABLE III: Local prediction performance on KonIQ [31]. All methods are conducted using identical training and testing protocol. The best results are highlighted in bold.

SROCC	Excellent	Good	Fair	Poor	Bad
DBCNN [56]	0.125	0.699	0.654	0.322	-
MetaIQA [67]	0.167	0.645	0.560	0.574	-
HyperIQA [70]	0.133	0.688	0.624	0.517	0.598
REQA	0.152	0.751	0.665	0.722	0.571
PLCC	Excellent	Good	Fair	Poor	Bad
DBCNN [56]	0.293	0.702	0.657	0.363	0.180
MetaIQA [67]	0.289	0.640	0.567	0.585	0.507
HyperIQA [70]	0.311	0.688	0.629	0.563	0.570
REQA	0.435	0.746	0.660	0.768	0.851

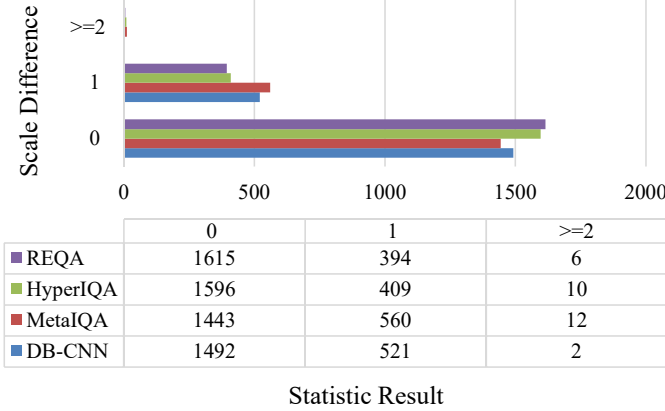


Fig. 6: Statistics of prediction deviation on a wide range.

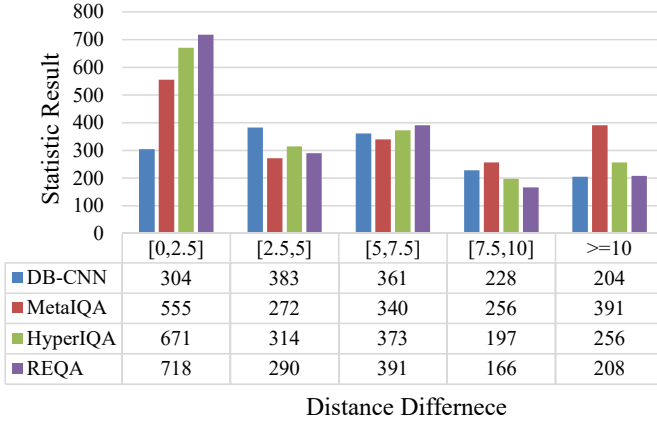


Fig. 7: Statistics of prediction deviation in a micro range.

this case, REQA still keeps competitive. In *Excellent* range, REQA achieves the best result on PLCC and the second-best result on SROCC. The same is true in *Bad* range.

2) *Outlier and deviation analysis*: To further verify the effectiveness of REQA, we make statistic analysis between pMOS and the ground truth. As is shown in Fig.5, we depicts the experimental results for a direct visualization. On the whole, the linear fitting of the predicted results of REQA is more similar to the directly proportional function compared to DBCNN [56] and HyperIQA [70]. Compared to

TABLE IV: SROCC results of the cross-database evaluations. The experiment is conducted by training on one database and testing on the full of another database.

	Testing	PQR [72]	DBCNN [56]	HyperIQA [70]	REQA
CLIVE	BID	0.714	0.762	0.756	0.825
	KonIQ	0.757	0.754	0.772	0.762
BID	CLIVE	0.680	0.725	0.770	0.747
	KonIQ	0.636	0.724	0.688	0.699
KonIQ	CLIVE	0.770	0.755	0.785	0.772
	BID	0.755	0.816	0.819	0.833

MetaIQA [67], though REQA fails to achieve better linear fitting function, the distribution of its predicted results is more concentrated. This demonstrates that the results of REQA possess the best linear correlation with the ground truth data on a wide range. Moreover, focusing on a particular range (e.g. points within green box), the results of REQA keep the same property. In addition, compared to the other methods, the predicted outliers (e.g. points within green boxes) of REQA is more close to the fitting curve. This means that REQA can alleviate the prediction deviation from a wide range effectively.

To further examine this visual analysis, the prediction deviation of different scales is quantified as is illustrated in Fig.6. Here, x-axis represents the statistic result and y-axis is the scale difference between pMOS and MOS. It is obvious that REQA is capable of limiting more images to its original quality scale and meantime it can reduce the wide range of prediction deviation as much as possible.

In addition, we also quantify the prediction deviation in micro ranges which is shown in Fig.7. Here, x-axis refers to the difference range of pMOS and MOS, and y-axis depicts the number of the samples. Compared to the other methods, REQA achieves the best performance as there are 718 samples in [0, 2.5] and the most prediction biases concentrate in the first three ranges. This means that the predicted scores of REQA possess smaller fluctuation, and furthermore demonstrates that the multi-level fine-grained losses is able to perceive minor changes of image quality.

D. Generalization Ability Test

In order to explore the generalization ability of the proposed model, we run cross database tests on authentically distorted IQA databases compared with the other three methods PQR [72], DBCNN [56] and HyperIQA [70].

The experiment is conducted by training on one database and testing on the full of another database. As we can see in Tab.IV, the proposed method achieves outstanding generalization ability as it obtains the best results twice and four top-two results. Especially, compared to HyperIQA [56], REQA achieves 6.3% improvement on SROCC when trained on CLIVE and tested on BID. Overall, the performance of REQA is a slightly lower than HyperIQA [70]. The reason for this is that the self-adaptive strategy makes it effective to assess the image quality according to content information. In the case that the scene changes, it can quickly perceive this

TABLE V: Ablation Experiments about the performance of each module. Here, we compare the gains of BL, GCMU and LDPM based on the global prediction performance.

CLIVE	SROCC	PLCC
REQA w/o FN+TE	0.830	0.854
REQA w/o FN	0.851	0.871
REQA w/o TE	0.843	0.847
REQA	0.865	0.880

TABLE VI: Ablation Experiments about the effectiveness of coarse-grained loss and fine-grained loss. The comparison is conducted based on the local prediction performance.

SROCC	Excellent	Good	Fair	Poor	Bad
REQA w/o L^{Coarse}	0.713	0.528	0.316	0.066	0.608
REQA	0.4393	0.620	0.504	0.511	0.674
PLCC	Excellent	Good	Fair	Poor	Bad
REQA w/o L^{Coarse}	0.768	0.525	0.384	0.143	0.707
REQA	0.0.911	0.611	0.555	0.551	0.659

change. The advantage reminds us to perfect the proposed method through improve the adaptability in the future work.

E. Ablation Study

In this section, we make ablation experiments to verify the contribution of key constituent parts of REQA. We conduct the ablation experiments on CLIVE. The training and testing protocols are the same as above.

We firstly examine the gains of three modules, the baseline network **ResNet50**, **FN** and **TE**. The results is listed in Tab.V. The modified model only removes respective module and the loss function is not changed. Specifically, in model **REQA w/o FN+TE**, the baseline network (**BL**) **ResNet50** [12] is left to predict the image quality to get about 0.830 on PLCC and 0.854 on PLCC. Compare to **BL**, model **REQA w/o TE** achieves 10% improvement on SROCC which proves the effectiveness of feedback module. And in model **REQA w/o FN**, about 0.851 on SROCC and 0.871 on PLCC is obtained. This demonstrates that global context feature is quality-aware to improve the assessment performance. Model **REQA** achieves the best results, which illustrates that modules interact with each other to get a positive gain.

Then we analyze the effectiveness of L^{Fine} and L^{Coarse} which is shown in Tab.VI. According to local performance comparison, we can conclude that **REQA**+ L^{Fine} guarantees the prominent performance of the algorithm. And L^{Coarse} is favorable for **REQA** to obtain ideal results in narrow ranges.

Overall, we can make the subsequent conclusions. First of all, different modules proposed in this paper can improve the performance of **REQA**. **TE** enlarges the receptive field to acquire the context features. **FN** can obtain more quality-aware perception of multi-scale features while completing the task iterations. L^{Fine} makes **REQA** have a prediction accuracy and with the addition of L^{Coarse} , local prediction performance gets promoted. All of these are responsible for the outstanding experimental results of **REQA**.

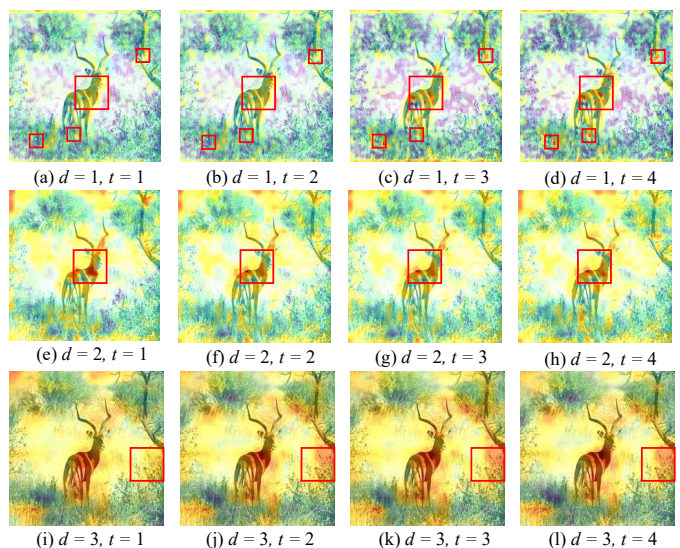


Fig. 8: Visualization of the local distortion information in the form of the heat map.

F. Visualization of Local Distortion Features

In this section, we visualize the local distortion information in the form of the heat map [76] to further examine the performance of the feedback hierarchy. We show each heat map corresponding to the output of $d'th$ feedback block in $t'th$ time step in Fig.8. Here, the displayed image 12949713.jpg is from KonIQ [31]. As we can see from the longitudinal comparison, different feedback blocks possess different receptive fields. For example, through comparing Fig.8(a), (e) and (i), it can be concluded that the third feedback block perceives larger areas where the textures is much clearer. This is attributed to different scales of inputs of three feedback blocks. Furthermore, by horizontal comparison, it can be concluded that feedback blocks can obtained more fine-grained feature maps which is consistent with our standpoint. For example, through making comparisons of Fig.8 (a)-(d), we can see that heat map in $t = 4$ has more heat sensitive areas (e.g. points within green boxes). In addition, we obtain the pMOS of the image in each time step as 79.01 in $t = 1$, 82.02 in $t = 2$, 83.16 in $t = 3$, and 82.13 in $t = 4$. The MOS of it is 84.91. This means that with the feedback going on, REQA can make more accurate prediction. Overall, we can conclude that the feedback hierarchy can achieves better and better features as iteration goes on. These features are quality-aware enough to ensure REQA obtain more fine-grained prediction result.

V. CONCLUSION

In this paper, we first propose the coarse-to-fine method to tackle the range effect in BIQA. Benefitting from FN and TE, the proposed method can perceive the multi-scale distortion information and global context information, which makes the model quality-aware. Furthermore, fusing coarse-grained metric and fin-grained losses into the feedback hierarchy to process these features, the proposed method achieves outstanding global and local prediction performance as is demonstrated by a series of experimental results.

REFERENCES

- [1] L. Krasula, K. Fliegel, P. Le Callet, and M. Klíma, "On the accuracy of objective image and video quality models: New methodology for performance evaluation," in *2016 Eighth International Conference on Quality of Multimedia Experience (QoMEX)*, 2016, pp. 1–6.
- [2] L. Krasula, P. Le Callet, K. Fliegel, and M. Klíma, "Quality assessment of sharpened images: Challenges, methodology, and objective metrics," *IEEE Transactions on Image Processing*, vol. 26, no. 3, pp. 1496–1508, 2017.
- [3] Z. Wang, A. C. Bovik, H. R. Sheikh, E. P. Simoncelli *et al.*, "Image quality assessment: from error visibility to structural similarity," *IEEE Transactions on Image Processing*, vol. 13, no. 4, pp. 600–612, 2004.
- [4] Z. Wang and A. C. Bovik, "Mean squared error: Love it or leave it? a new look at signal fidelity measures," *IEEE signal processing magazine*, vol. 26, no. 1, pp. 98–117, 2009.
- [5] D. P. Kingma and J. Ba, "Adam: A method for stochastic optimization," *arXiv preprint arXiv:1412.6980*, 2014.
- [6] K. Ma, Q. Wu, Z. Wang, Z. Duanmu, H. Yong, H. Li, and L. Zhang, "Group mad competition—a new methodology to compare objective image quality models," in *Proceedings of the IEEE Conference on Computer Vision and Pattern Recognition*, 2016, pp. 1664–1673.
- [7] Q. Wu, H. Li, K. N. Ngan, and K. Ma, "Blind image quality assessment using local consistency aware retriever and uncertainty aware evaluator," *IEEE Transactions on Circuits and Systems for Video Technology*, vol. 28, no. 9, pp. 2078–2089, 2018.
- [8] Q. Jiang, F. Shao, W. Lin, and G. Jiang, "Blique-tmi: Blind quality evaluator for tone-mapped images based on local and global feature analyses," *IEEE Transactions on Circuits and Systems for Video Technology*, vol. 29, no. 2, pp. 323–335, 2019.
- [9] Q. Wu, H. Li, F. Meng, K. N. Ngan, B. Luo, C. Huang, and B. Zeng, "Blind image quality assessment based on multichannel feature fusion and label transfer," *IEEE Transactions on Circuits and Systems for Video Technology*, vol. 26, no. 3, pp. 425–440, 2016.
- [10] Y. Chen, Y. Zhao, S. Li, W. Zuo, W. Jia, and X. Liu, "Blind quality assessment for cartoon images," *IEEE Transactions on Circuits and Systems for Video Technology*, vol. 30, no. 9, pp. 3282–3288, 2020.
- [11] R. I.-R. BT, "Methodology for the subjective assessment of the quality of television pictures," *International Telecommunication Union*, 2002.
- [12] K. He, X. Zhang, S. Ren, and J. Sun, "Deep residual learning for image recognition," in *Proceedings of the IEEE conference on computer vision and pattern recognition*, 2016, pp. 770–778.
- [13] S. Xingjian, Z. Chen, H. Wang, D.-Y. Yeung, W.-K. Wong, and W.-c. Woo, "Convolutional lstm network: A machine learning approach for precipitation nowcasting," in *Advances in neural information processing systems*, 2015, pp. 802–810.
- [14] C. Finn, P. Abbeel, and S. Levine, "Model-agnostic meta-learning for fast adaptation of deep networks," in *International Conference on Machine Learning*, 2017, pp. 1126–1135.
- [15] A. Vaswani, N. Shazeer, N. Parmar, J. Uszkoreit, L. Jones, A. N. Gomez, E. Kaiser, and I. Polosukhin, "Attention is all you need," in *Advances in neural information processing systems*, 2017, pp. 5998–6008.
- [16] J. Devlin, M.-W. Chang, K. Lee, and K. Toutanova, "Bert: Pre-training of deep bidirectional transformers for language understanding," *arXiv preprint arXiv:1810.04805*, 2018.
- [17] A. Dosovitskiy, L. Beyer, A. Kolesnikov, D. Weissenborn, X. Zhai, T. Unterthiner, M. Dehghani, M. Minderer, G. Heigold, S. Gelly *et al.*, "An image is worth 16x16 words: Transformers for image recognition at scale," *arXiv preprint arXiv:2010.11929*, 2020.
- [18] H. R. Sheikh and A. C. Bovik, "Image information and visual quality," *IEEE Transactions on image processing*, vol. 15, no. 2, pp. 430–444, 2006.
- [19] W. Xue, L. Zhang, X. Mou, and A. C. Bovik, "Gradient magnitude similarity deviation: A highly efficient perceptual image quality index," *IEEE Transactions on Image Processing*, vol. 23, no. 2, pp. 684–695, 2013.
- [20] L. Zhang, L. Zhang, X. Mou, and D. Zhang, "Fsim: A feature similarity index for image quality assessment," *IEEE transactions on Image Processing*, vol. 20, no. 8, pp. 2378–2386, 2011.
- [21] L. Ma, S. Li, F. Zhang, and K. N. Ngan, "Reduced-reference image quality assessment using reorganized dct-based image representation," *IEEE Transactions on multimedia*, vol. 13, no. 4, pp. 824–829, 2011.
- [22] G. Zhai, X. Wu, X. Yang, W. Lin, and W. Zhang, "A psychovisual quality metric in free-energy principle," *IEEE Transactions on Image Processing*, vol. 21, no. 1, pp. 41–52, 2011.
- [23] A. Rehman and Z. Wang, "Reduced-reference image quality assessment by structural similarity estimation," *IEEE transactions on image processing*, vol. 21, no. 8, pp. 3378–3389, 2012.
- [24] L. Krasula, K. Fliegel, P. Le Callet, and M. Klíma, "On the accuracy of objective image and video quality models: New methodology for performance evaluation," in *2016 Eighth International Conference on Quality of Multimedia Experience (QoMEX)*, 2016, pp. 1–6.
- [25] H. R. Sheikh, M. F. Sabir, and A. C. Bovik, "A statistical evaluation of recent full reference image quality assessment algorithms," *IEEE Transactions on Image Processing*, vol. 15, no. 11, pp. 3440–3451, 2006.
- [26] D. Jayaraman, A. Mittal, A. K. Moorthy, and A. C. Bovik, "Objective quality assessment of multiply distorted images," in *2012 Conference record of the forty sixth asilomar conference on signals, systems and computers (ASILOMAR)*, 2012, pp. 1693–1697.
- [27] N. Ponomarenko, L. Jin, O. Ieremeiev, V. Lukin, K. Egiazarian, J. Astola, B. Vozel, K. Chehdi, M. Carli, F. Battisti *et al.*, "Image database tid2013: Peculiarities, results and perspectives," *Signal Processing: Image Communication*, vol. 30, pp. 57–77, 2015.
- [28] E. C. Larson and D. M. Chandler, "Most apparent distortion: full-reference image quality assessment and the role of strategy," *Journal of Electronic Imaging*, vol. 19, no. 1, p. 011006, 2010.
- [29] H. Lin, V. Hosu, and D. Saupe, "Kadid-10k: A large-scale artificially distorted iqa database," in *2019 Eleventh International Conference on Quality of Multimedia Experience (QoMEX)*, 2019, pp. 1–3.
- [30] D. Ghadiyaram and A. C. Bovik, "Massive online crowdsourced study of subjective and objective picture quality," *IEEE Transactions on Image Processing*, vol. 25, no. 1, pp. 372–387, 2016.
- [31] V. Hosu, H. Lin, T. Sziranyi, and D. Saupe, "KonIQ-10k: An ecologically valid database for deep learning of blind image quality assessment," *IEEE Transactions on Image Processing*, vol. 29, pp. 4041–4056, 2020.
- [32] A. Ciancio, E. A. da Silva, A. Said, R. Samadani, P. Obrador *et al.*, "No-reference blur assessment of digital pictures based on multifeature classifiers," *IEEE Transactions on image processing*, vol. 20, no. 1, pp. 64–75, 2010.
- [33] M. A. Saad, P. Le Callet, and P. Corriceau, "Blind image quality assessment: Unanswered questions and future directions in the light of consumers needs," *VQEG eLetter*, vol. 1, no. 2, pp. 62–66, 2014.
- [34] Z. Ying, H. Niu, P. Gupta, D. Mahajan, D. Ghadiyaram, and A. Bovik, "From patches to pictures (paq-2-piq): Mapping the perceptual space of picture quality," in *Proceedings of the IEEE/CVF Conference on Computer Vision and Pattern Recognition*, 2020, pp. 3575–3585.
- [35] M. H. Pinson and S. Wolf, "A new standardized method for objectively measuring video quality," *IEEE Transactions on broadcasting*, vol. 50, no. 3, pp. 312–322, 2004.
- [36] B. Kulis *et al.*, "Metric learning: A survey," *Foundations and trends in machine learning*, vol. 5, no. 4, pp. 287–364, 2012.
- [37] A. Bellet, A. Habrard, and M. Sebban, "Metric learning," *Synthesis Lectures on Artificial Intelligence and Machine Learning*, vol. 9, no. 1, pp. 1–151, 2015.
- [38] F. Gao, Y. Wang, P. Li, M. Tan, J. Yu, and Y. Zhu, "Deepsim: Deep similarity for image quality assessment," *Neurocomputing*, vol. 257, pp. 104–114, 2017.
- [39] E. Prashnani, H. Cai, Y. Mostofi, and P. Sen, "Pieapp: Perceptual image-error assessment through pairwise preference," in *Proceedings of the IEEE Conference on Computer Vision and Pattern Recognition*, 2018, pp. 1808–1817.
- [40] X. Liu, J. van de Weijer, and A. D. Bagdanov, "Rankika: Learning from rankings for no-reference image quality assessment," in *Proceedings of the IEEE International Conference on Computer Vision*, 2017, pp. 1040–1049.
- [41] R. L. Goldstone, "Perceptual learning," *Annual review of psychology*, vol. 49, no. 1, pp. 585–612, 1998.
- [42] S. Hochstein and M. Ahissar, "View from the top: Hierarchies and reverse hierarchies in the visual system," *Neuron*, vol. 36, no. 5, pp. 791–804, 2002.
- [43] A. R. Zamir, T.-L. Wu, L. Sun, W. B. Shen, B. E. Shi, J. Malik, and S. Savarese, "Feedback networks," in *Proceedings of the IEEE Conference on Computer Vision and Pattern Recognition*, 2017, pp. 1308–1317.
- [44] A. K. Moorthy and A. C. Bovik, "Blind image quality assessment: From natural scene statistics to perceptual quality," *IEEE transactions on Image Processing*, vol. 20, no. 12, pp. 3350–3364, 2011.
- [45] M. A. Saad, A. C. Bovik, and C. Charrier, "Blind image quality assessment: A natural scene statistics approach in the dct domain," *IEEE transactions on Image Processing*, vol. 21, no. 8, pp. 3339–3352, 2012.

- [46] A. Mittal, A. K. Moorthy, and A. C. Bovik, "No-reference image quality assessment in the spatial domain," *IEEE Transactions on image processing*, vol. 21, no. 12, pp. 4695–4708, 2012.
- [47] Q. Li, W. Lin, J. Xu, and Y. Fang, "Blind image quality assessment using statistical structural and luminance features," *IEEE Transactions on Multimedia*, vol. 18, no. 12, pp. 2457–2469, 2016.
- [48] Q. Wu, Z. Wang, and H. Li, "A highly efficient method for blind image quality assessment," in *2015 IEEE International Conference on Image Processing (ICIP)*, 2015, pp. 339–343.
- [49] T. Dai, K. Gu, L. Niu, Y.-b. Zhang, W. Lu, and S.-T. Xia, "Referenceless quality metric of multiply-distorted images based on structural degradation," *Neurocomputing*, vol. 290, pp. 185–195, 2018.
- [50] L. Li, W. Xia, W. Lin, Y. Fang, and S. Wang, "No-reference and robust image sharpness evaluation based on multiscale spatial and spectral features," *IEEE Transactions on Multimedia*, vol. 19, no. 5, pp. 1030–1040, 2016.
- [51] P. Ye and D. Doermann, "No-reference image quality assessment using visual codebooks," *IEEE Transactions on Image Processing*, vol. 21, no. 7, pp. 3129–3138, 2012.
- [52] P. Ye, J. Kumar, L. Kang, and D. Doermann, "Unsupervised feature learning framework for no-reference image quality assessment," in *2012 IEEE Conference on Computer Vision and Pattern Recognition*, 2012, pp. 1098–1105.
- [53] L. Kang, P. Ye, Y. Li, and D. Doermann, "Convolutional neural networks for no-reference image quality assessment," in *Proceedings of the IEEE Conference on Computer Vision and Pattern Recognition*, 2014, pp. 1733–1740.
- [54] S. Bosse, D. Maniry, K.-R. Müller, T. Wiegand, and W. Samek, "Deep neural networks for no-reference and full-reference image quality assessment," *IEEE Transactions on image processing*, vol. 27, no. 1, pp. 206–219, 2017.
- [55] K. Ma, W. Liu, K. Zhang, Z. Duanmu, Z. Wang, and W. Zuo, "End-to-end blind image quality assessment using deep neural networks," *IEEE Transactions on Image Processing*, vol. 27, no. 3, pp. 1202–1213, 2018.
- [56] W. Zhang, K. Ma, J. Yan, D. Deng, and Z. Wang, "Blind image quality assessment using a deep bilinear convolutional neural network," *IEEE Transactions on Circuits and Systems for Video Technology*, vol. 30, no. 1, pp. 36–47, 2018.
- [57] K. Ma, W. Liu, T. Liu, Z. Wang, and D. Tao, "dipiq: Blind image quality assessment by learning-to-rank discriminable image pairs," *IEEE Transactions on Image Processing*, vol. 26, no. 8, pp. 3951–3964, 2017.
- [58] J. Gu, G. Meng, C. Da, S. Xiang, and C. Pan, "No-reference image quality assessment with reinforcement recursive list-wise ranking," in *Proceedings of the AAAI Conference on Artificial Intelligence*, vol. 33, no. 01, 2019, pp. 8336–8343.
- [59] J. Kim, A.-D. Nguyen, and S. Lee, "Deep cnn-based blind image quality predictor," *IEEE transactions on neural networks and learning systems*, vol. 30, no. 1, pp. 11–24, 2018.
- [60] D. Pan, P. Shi, M. Hou, Z. Ying, S. Fu, and Y. Zhang, "Blind predicting similar quality map for image quality assessment," in *Proceedings of the IEEE conference on computer vision and pattern recognition*, 2018, pp. 6373–6382.
- [61] O. Ronneberger, P. Fischer, and T. Brox, "U-net: Convolutional networks for biomedical image segmentation," in *International Conference on Medical image computing and computer-assisted intervention*, 2015, pp. 234–241.
- [62] S. Seo, S. Ki, and M. Kim, "Deep hvs-iqa net: Human visual system inspired deep image quality assessment networks," *arXiv preprint arXiv:1902.05316*, 2019.
- [63] K.-Y. Lin and G. Wang, "Hallucinated-iqa: No-reference image quality assessment via adversarial learning," in *Proceedings of the IEEE Conference on Computer Vision and Pattern Recognition*, 2018, pp. 732–741.
- [64] H. Ren, D. Chen, and Y. Wang, "Ran4iqa: Restorative adversarial nets for no-reference image quality assessment," in *Thirty-Second AAAI Conference on Artificial Intelligence*, 2018.
- [65] F. Gao, J. Yu, S. Zhu, Q. Huang, and Q. Tian, "Blind image quality prediction by exploiting multi-level deep representations," *Pattern Recognition*, vol. 81, pp. 432–442, 2018.
- [66] J. Deng, W. Dong, R. Socher, L.-J. Li, K. Li, and L. Fei-Fei, "Imagenet: A large-scale hierarchical image database," in *2009 IEEE conference on computer vision and pattern recognition*, 2009, pp. 248–255.
- [67] H. Zhu, L. Li, J. Wu, W. Dong, and G. Shi, "Metaiqa: Deep meta-learning for no-reference image quality assessment," in *Proceedings of the IEEE/CVF Conference on Computer Vision and Pattern Recognition*, 2020, pp. 14 143–14 152.
- [68] Y. Bengio, J. Louradour, R. Collobert, and J. Weston, "Curriculum learning," in *Proceedings of the 26th annual international conference on machine learning*, 2009, pp. 41–48.
- [69] D. Li, T. Jiang, W. Lin, and M. Jiang, "Which has better visual quality: The clear blue sky or a blurry animal?" *IEEE Transactions on Multimedia*, vol. 21, no. 5, pp. 1221–1234, 2018.
- [70] S. Su, Q. Yan, Y. Zhu, C. Zhang, X. Ge, J. Sun, and Y. Zhang, "Blindly assess image quality in the wild guided by a self-adaptive hyper network," in *Proceedings of the IEEE/CVF Conference on Computer Vision and Pattern Recognition*, 2020, pp. 3667–3676.
- [71] Y. Liang, J. Wang, X. Wan, Y. Gong, and N. Zheng, "Image quality assessment using similar scene as reference," in *European Conference on Computer Vision*, 2016, pp. 3–18.
- [72] H. Zeng, L. Zhang, and A. C. Bovik, "Blind image quality assessment with a probabilistic quality representation," in *2018 25th IEEE International Conference on Image Processing (ICIP)*. IEEE, 2018, pp. 609–613.
- [73] D. Varga, D. Saupe, and T. Szirányi, "Deepn: A content preserving deep architecture for blind image quality assessment," in *2018 IEEE International Conference on Multimedia and Expo (ICME)*, 2018, pp. 1–6.
- [74] K. Ma, Z. Duanmu, Q. Wu, H. Yong, H. Li, and L. Zhang, "Waterloo exploration database: New challenges for image quality assessment models," *IEEE Transactions on Image Processing*, vol. 26, no. 2, pp. 1004–1016, 2017.
- [75] J. Ma, J. Wu, L. Li, W. Dong, X. Xie, G. Shi, and W. Lin, "Blind image quality assessment with active inference," *IEEE Transactions on Image Processing*, vol. 30, pp. 3650–3663, 2021.
- [76] R. R. Selvaraju, M. Cogswell, A. Das, R. Vedantam, D. Parikh, and D. Batra, "Grad-cam: Visual explanations from deep networks via gradient-based localization," in *Proceedings of the IEEE international conference on computer vision*, 2017, pp. 618–626.
- [77] J. Xu, P. Ye, Q. Li, H. Du, Y. Liu, and D. Doermann, "Blind image quality assessment based on high order statistics aggregation," *IEEE Transactions on Image Processing*, vol. 25, no. 9, pp. 4444–4457, 2016.
- [78] L. Zhang, L. Zhang, and A. C. Bovik, "A feature-enriched completely blind image quality evaluator," *IEEE Transactions on Image Processing*, vol. 24, no. 8, pp. 2579–2591, 2015.
- [79] J. Kim and S. Lee, "Fully deep blind image quality predictor," *IEEE Journal of selected topics in signal processing*, vol. 11, no. 1, pp. 206–220, 2016.
- [80] S. Yang, Q. Jiang, W. Lin, and Y. Wang, "Sgdnet: An end-to-end saliency-guided deep neural network for no-reference image quality assessment," in *Proceedings of the 27th ACM International Conference on Multimedia*, 2019, pp. 1383–1391.
- [81] S.-H. Bae and M. Kim, "A dct-based total jnd profile for spatiotemporal and foveated masking effects," *IEEE Transactions on Circuits and Systems for Video Technology*, vol. 27, no. 6, pp. 1196–1207, 2016.